Mon. Not. R. Astron. Soc. **304,** 540–548 (1999)

Stellar populations and ages of M82 super star clusters

John S. Gallagher, III[1]★ and Linda J. Smith[2]★

[1]*Department of Astronomy, University of Wisconsin-Madison, 5534 Sterling, 475 North Charter Street, Madison, WI 53706, USA*
[2]*Department of Physics and Astronomy, University College London, Gower Street, London WC1E 6BT*

Accepted 1998 November 30. Received 1998 November 23; in original form 1998 August 28

ABSTRACT

We present high signal-to-noise ratio optical spectra of two luminous super star clusters in the starburst galaxy M82. The data for cluster F and the nearby, highly reddened, cluster L were obtained with the William Herschel Telescope (WHT) at a resolution of 1.6 Å. The blue spectrum (3250–5540 Å) of cluster F shows features typical of mid-B stars. The red spectra (5730–8790 Å) of clusters F and L show the Ca II triplet and numerous F- and G-type absorption features. Strong Ca II and Na I interstellar absorption lines arising in M82 are also detected, and the λ6283 diffuse interstellar band appears to be present. The quality of the WHT spectra allows us to improve previous age estimates considerably for cluster F. By comparing the blue spectrum with theoretical model cluster spectra using the PEGASE spectral synthesis code, we derive an age of 60 ± 20 Myr. The strength of the Ca II triplet is also in accord with this age. Cluster L appears to have a similar age, although this is much less certain. The measured radial velocities for the two clusters differ substantially, indicating that they are located in different regions of the M82 disc. Cluster F appears to be deep in M82, slightly beyond the main starburst region, while the highly obscured cluster L lies near the outer edges of the disc. We derive an absolute magnitude $M_V = -16.5$ for F, indicating that it is an extremely massive cluster. The presence of such a luminous super star cluster suggests that the M82 starburst experienced an episode of intense star formation ≈60 Myr ago.

Key words: galaxies: evolution – galaxies: individual: M82 – galaxies: starburst – galaxies: star clusters – galaxies: stellar content.

1 INTRODUCTION

M82 is one of the nearest examples of a spectacular starburst galaxy. At a distance of 3.6 Mpc (see Freedman et al. 1994) its far-infrared luminosity is about $3.2 \times 10^{10}\,L_\odot$ (Colbert et al. 1999), and the many effects of the starburst, including extreme optical surface brightness and giant outflows, are immediately apparent (e.g. Lynds & Sandage 1963). M82 has naturally played a special role in studies of intense star formation on large scales (e.g. Telesco 1988). Among the results from ground-based optical and infrared investigations of M82 was the recognition that dense, luminous star clusters are common in M82 (O'Connell & Mangano 1978, hereafter OM78). High angular resolution optical imaging with the Wide Field Planetary Camera on the *Hubble Space Telescope* (*HST*) revealed more than 100 clusters located in the optically visible skin of the M82 starburst region (O'Connell et al. 1995). Infrared imaging penetrates the dense gas and dust in the starburst and finds populations of compact, luminous star clusters in the actively star-forming regions of the galaxy (Satyapal et al. 1995, 1997). Star clusters are evidently a featured product of the intense star formation now occurring within M82. This is consistent with the more extensive results from the *HST* showing compact, luminous 'super star clusters' (SSCs) to be frequently associated with starbursts under a wide range of conditions (e.g. Whitmore et al. 1993; Conti & Vacca 1994; O'Connell, Gallagher & Hunter 1994; Whitmore & Schweizer 1995; Meurer et al. 1995; Schweizer et al. 1996; see Ho 1997 for a review).

The presence of super star clusters in starburst galaxies provides us with a useful tool for exploring some aspects of at least their recent star formation histories, while also yielding some information about chemical abundances in stars. These measurements are feasible because star clusters closely approximate a coeval, single-metallicity, simple stellar population (SSP). An SSP is the simplest class of stellar system to model, and one in which age and metallicity can be extracted from the integrated spectrum (see Bruzual & Charlot 1993; Bruzual 1996). In return for their increased complexity, SSCs offer several practical advantages as compared with observations of individual stars; most significantly they can be 10–100 or more times as luminous as the brightest supergiant stars, allowing SSCs to be observed at greater distances or against more complex backgrounds.

Achieving the potential of SSCs as astrophysical probes of starburst galaxies, however, has proven difficult. Starbursts are often dusty, limiting the utility of optical and ultraviolet colours

★E-mail: jsg@astro.wisc.edu (JSG); ljs@star.ucl.ac.uk (LJS)

to yield ages of younger clusters (e.g. Watson et al. 1996). For intermediate age or older star clusters the well-known age–metallicity degeneracy becomes an issue (Searle, Wilkinson & Bagnuolo 1980). Optical and ultraviolet spectra are available for a few blue SSCs, but initial studies were limited to qualitative discussions (e.g. Arp & Sandage 1985; Lamb et al. 1985). More recent observations have led to considerable progress in analysing very young SSCs, where strengths and profiles of ultraviolet atomic resonance lines are powerful diagnostics (e.g. Vacca et al. 1995; González Delgado, Leitherer & Heckman 1997).

Optically luminous SSCs tend to be dominated in the blue by B- or A-type spectra (Schweizer & Seitzer 1993; Zepf et al. 1995; Brodie et al. 1998). As a result, ages are not readily determined from measurements of individual spectral features, especially when the Balmer jump is not available (Diaz 1988). In addition, these studies have found that the observed strengths of the Balmer lines exceed those predicted by the Bruzual & Charlot (1993) models. Brodie et al. (1998) find that a truncated initial mass function (IMF) is needed to reproduce their observations of the galaxy NGC 1275. For the M82 starburst, Satyapal et al. (1997) use a wealth of infrared data to infer a typical age of 10^7 yr for the clusters within a radius of 250 pc of the nucleus. They also find an age dispersion of 6×10^6 yr, which is correlated with the projected distance of the clusters from the nucleus, and therefore suggest that the starburst is propagating outwards from the nucleus.

In this paper we present a new spectroscopic study of the luminous SSC F in M82 (OM78) and the nearby, highly reddened, cluster L (Kronberg, Pritchet & van den Bergh 1972). Cluster F has a size of about 9×5 pc from observations with the original Planetary Camera on *HST* and an estimated luminosity of $M_V^0 \approx -14.5$ (O'Connell et al. 1995), and is therefore one of the most luminous younger star clusters known. It is located 25 arcsec (= 440 pc) south-west of the 2.2-μm nucleus and is considered to be in a less obscured region of the starburst (O'Connell et al. 1995). The goal of our programme is to develop improved approaches for quantitatively matching spectra of SSCs to model predictions as a means to determine cluster ages. Observations for this project were made at the 4.2-m William Herschel Telescope (WHT) using the double-beam spectrograph ISIS. This allowed us to obtain wide wavelength coverage with good spectral resolution, and thereby considerably improve the estimated age for cluster F.

The observational procedures are reviewed in the next section. In Section 3 we describe the spectra, while Section 4 compares observed spectra with predictions from a population synthesis model. Results are discussed in Section 5, including implications for the duration of the M82 starburst and the quality of current models for SSPs with near-solar metallicity.

2 OBSERVATIONS AND DATA REDUCTION

Observations of SSC F in M82 were obtained on 1997 March 25/26 with the WHT on La Palma, Canary Islands. SSC F was observed at a position angle of 20° so that spectra of SSC L could also be obtained. The journal of observations is given in Table 1. The double-beam spectrograph ISIS was used with Tektronix charge-coupled devices (CCDs) (1024×1024 24-μm pixels) on both the blue and red arms. Two 600-line gratings were used to give a continuous wavelength coverage from 3234 to 5537 Å and from 5726 to 8785 Å. A long slit of dimensions $1\farcs0\times4\farcm0$ was chosen to give a two-pixel spectral resolution of 1.6 Å. The spatial scale was $0\farcs36\,\mathrm{pixel}^{-1}$ and an average seeing of $1\farcs2$ was measured over the period of the observations.

Table 1. Journal of WHT observations.

Blue Arm		Red Arm	
Wavelength Range (Å)	Exposure Time (s)	Wavelength Range (Å)	Exposure Time (s)
3234–4042	2400	5726–6534	1200
		6478–7286	1200
3984–4792	1200	7224–8032	1200
4729–5537	2400	7977–8785	2400

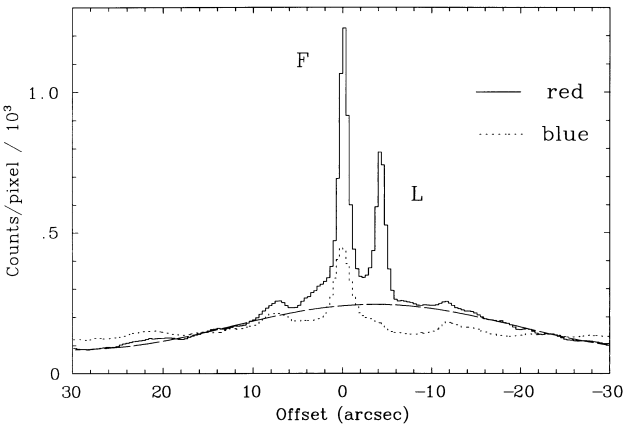

Figure 1. The raw spatial profiles for the red wavelength region (8100–8600 Å; solid line) and the blue region (4100–4600 Å; dotted line) normalized to the same exposure time. The two superclusters F and L are indicated. The *x*-axis represents the spatial offset with respect to the centre of SSC F and SSC L is 4 arcsec to the south-west of F. The dashed line shows a representation of the polynomial fit used to subtract off the underlying galaxy background for the red spectrum.

The data were reduced using the PAMELA optimal extraction routines (Horne 1986) within the FIGARO (Shortridge et al. 1997) software package. Each frame was first bias-corrected, and those obtained at the reddest wavelength setting were divided by a normalized flat field to remove the fringing. In Fig. 1, we show the spatial profile along the slit at representative red and blue wavelengths obtained by collapsing the raw images from 8100–8600 Å and 4100–4600 Å. It can be seen that SSC L is not detected in the blue region, and that there is a substantial contribution from the galaxy background. This was subtracted by using polynomial fits to each pixel in the spatial direction, as shown in Fig. 1. The object data were then optimally extracted and wavelength-calibrated using Cu–Ar comparison spectra taken before or after each integration. The red arm spectra were next corrected for telluric absorption features using a B star standard, and all spectra were extinction-corrected using the curve appropriate to La Palma.

Finally the data were flux-calibrated using the flux standard Feige 34 (Oke 1990) and the individual wavelength ranges were merged. To accomplish this, small adjustments of 5–15 per cent in flux level were required. The final spectra have a signal-to-noise ratio per pixel in the continuum of 30–40 above the Balmer jump for SSC F and longward of 7000 Å for SSC L.

3 DESCRIPTION OF SPECTRA

3.1 Continuum

In Figs 2 and 3 we show the flux-calibrated spectra for SSCs F and L

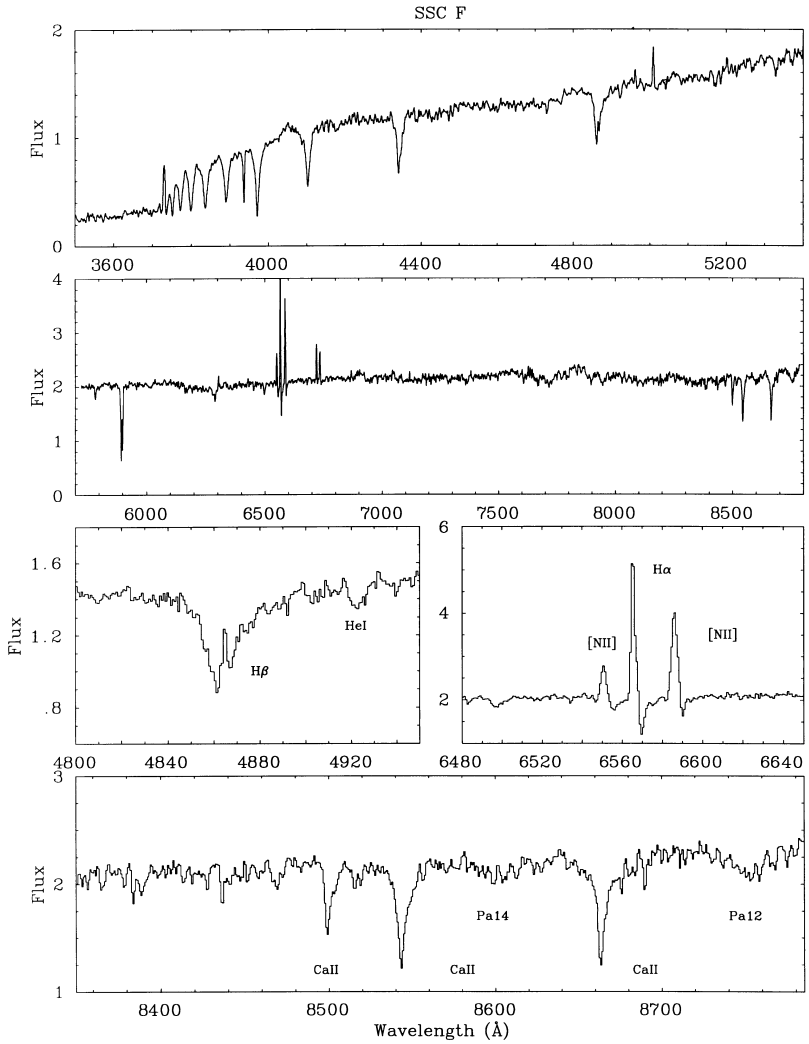

Figure 2. The blue and red spectra of SSC F (smoothed with $\sigma = 1.0$ Å for presentation purposes). The lower three boxes (at the full spectral resolution) show enlargements covering the Hβ, Hα + [N II], and Ca II triplet regions. The y-axis is in units of 10^{-15} erg s^{-1} cm^{-2} Å^{-1}.

and enlargements over selected wavelength ranges to highlight various spectral features. We have performed synthetic photometry on the spectra to derive magnitudes and colours. For SSC F, we derive *UBV* magnitudes of 17.6, 16.9 and 15.8 respectively giving $(U-B) = 0.70$ and $(B-V) = 1.07$. These colours are in excellent agreement with those of OM78 who derive $V = 15.00$, $(U-B) = 0.69$ and $(B-V) = 1.04$, using a 7″.5 aperture. From *HST* images, O'Connell et al. (1995) find $V = 16.3$ within a radius of 0″.5. For SSC L, we derive a monochromatic *R* magnitude of 16.7 compared to 15.6 for F.

3.2 Absorption lines

Line identifications, heliocentric velocities and equivalent widths of the principal spectral features are given in Table 2 for SSCs F and L. The equivalent widths were measured by defining continuum windows either side of the features, and the errors given in Table 2 represent 1σ uncertainties based on the signal-to-noise ratio in the continuum windows. We also list equivalent widths based on the windows defined by Bica & Alloin (1986), which tend to be much wider than the actual spectral features present in our data. We now discuss each SSC in turn.

3.2.1 M82 SSC F

The blue spectrum is dominated by broad Balmer absorption lines and a strong Balmer jump. Comparison of the equivalent widths of H9, H8 and Hδ (least likely to be affected by nebular emission) with main-sequence stars in the Jacoby, Hunter & Christian (1984) spectral library shows that the best match is for a mid-B spectral type. This classification is confirmed by the detection of weak He I lines (e.g. λ4922 to the red of Hβ in Fig. 2) and Mg II λ4481. We find that the strong and narrow Ca II K line arises from interstellar gas in M82 rather than stellar atmospheres since its velocity agrees with that of the Na I D lines and is very different from the stellar absorption features.

In the red spectrum, the strongest absorption features present belong to the Ca II triplet and we also detect broad absorption from members of the Paschen series. The equivalent widths given in Table 2 for the Ca II triplet have been measured using the continuum and line windows of Diaz, Terlevich & Terlevich (1989). The combined strength of the two strongest members (Ca2 + Ca3) is 8.5 Å, uncorrected for Paschen line absorption. The mean velocity of the triplet is $+35$ km s^{-1} and probably represents the most accurate value for the radial velocity of SSC F

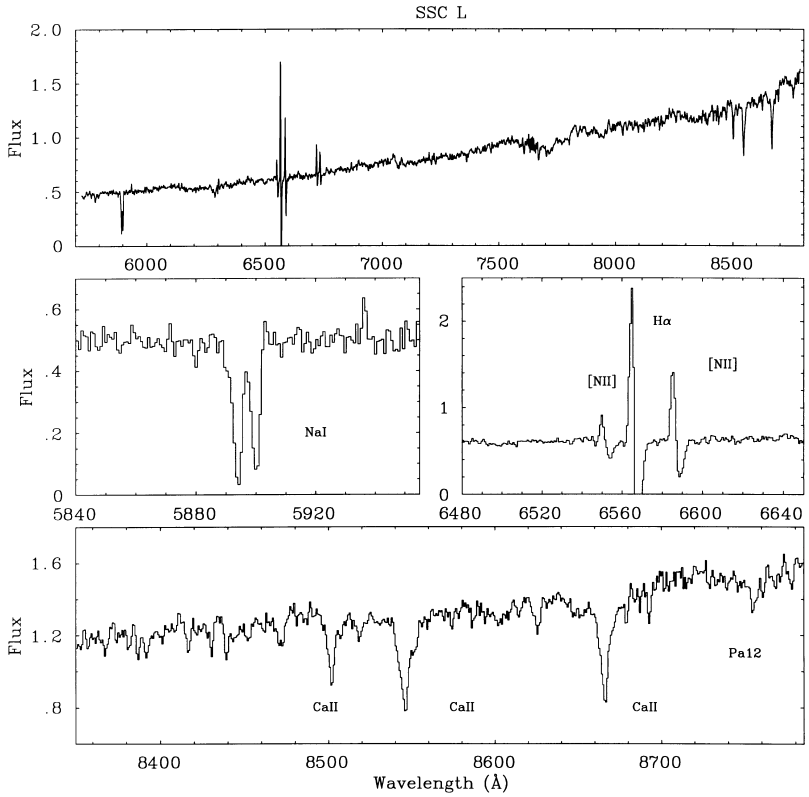

Figure 3. The red spectrum of SSC L (smoothed with $\sigma = 1.0$ Å for presentation purposes). The lower three boxes (at the full spectral resolution) show enlargements covering the Na I interstellar absorption lines, Hα + [N II], and Ca II triplet regions. The y-axis is in units of 10^{-15} erg s^{-1} cm^{-2} Å^{-1}.

since the Balmer lines are broad and contaminated by nebular emission.

The overall spectrum redward of 5000 Å has various features attributable to F and G stars (Andrillat, Jaschek & Jaschek 1995; Carquillat et al. 1997). In addition to the Ca II triplet, we detect weak absorption features due to Cr I + Cu I λ5782, Fe I + Ba II + Ca I λ6497 as well as various Ti I and Fe I lines near the Ca II triplet. No molecular bands due to e.g. TiO are detected in our spectra.

3.2.2 M82 SSC L

The red spectrum (Fig. 3) clearly shows that the Ca II triplet is present and a weak Pa 12 absorption line is detected, suggesting that blue stars are present in this cluster. Weak, low-ionization absorption features arising from F and G stars are also detected and have similar strengths to those found in F. The strengths of the Ca II triplet lines are similar to those measured for SSC L with Ca2 + Ca3 = 8.9 Å. The radial velocities are, however, quite different, with a mean for the Ca II triplet of +131 km s^{-1} compared to +35 km s^{-1} for F. This large difference in radial velocity indicates that clusters L and F lie at different locations along our sightline through the disc of M82.

3.3 Emission lines

For SSC F, we detect nebular emission lines of Hα, Hβ, Hγ, [O II] λ3727, 3729, [O III] λ4959, 5007, [O I] λ6300, [N II] λ6548, 6584, and [S II] λ6717, 6731. The Hβ and Hα + [N II] emission-line profiles are shown in Fig. 2, and heliocentric radial velocities and equivalent widths are given in Table 2. For the Hβ, Hγ, [O I], [O II] and [O III] lines, we derive a mean velocity of +181 ± 12 km s^{-1}, which agrees well with the mean velocity of the Ca II K and Na I D interstellar lines of +189 ± 5 km s^{-1}. The Hα, [N II] and [S II] lines show a lower velocity of +114 ± 9 km s^{-1} in good agreement with that determined by OM78 of +121 ± 10 km s^{-1} for the same features. Inspection of the images shows that the spatial structure of these lines is more complicated than the [O II] or [O III] emission, which is constant in intensity and velocity across the region displayed in Fig. 1. The emission for the strong Hα, [N II] and [S II] lines is clumpy with two velocity components – the component seen in the other lines at +181 km s^{-1} and another component at +114 km s^{-1}, which lies between SSCs F and L. As a result of this structure, the strong +181 km s^{-1} component is oversubtracted from both SSC spectra and appears in absorption in Figs 2 and 3.

For SSC L, we detect nebular emission lines of Hα, [N II] and [S II] and find compared to SSC F a lower mean heliocentric velocity of +69 ± 9 km s^{-1}. The equivalent widths of the nebular lines are similar for the two spectra.

3.4 Diffuse interstellar bands

Owing to their moderate to high levels of interstellar dust obscuration, M82 clusters F and L provide excellent sightlines for measuring interstellar features in the spectrum of M82. We have already noted the presence of strong interstellar absorption from the atomic species in the Ca II K and Na I D lines. Our spectra also have sufficient resolution and signal-to-noise ratios to allow sensitive searches for diffuse interstellar bands (DIBs). Major features of

Table 2. Velocity and equivalent width (W_λ) measurements.

Line	λ_{lab} (Å)	SSC F Velocity (km s^{-1})	SSC F Measured W_λ (Å)	SSC F Window[a] W_λ (Å)	SSC L Velocity (km s^{-1})	SSC L Measured W_λ (Å)	SSC L Window[a] W_λ (Å)	Comments
[O II]	3727	+176	−8.81 ± 0.21					Nebular
H12	3750.1	+41	3.03 ± 0.13					
H11	3770.6	+72	5.01 ± 0.16					
H10	3797.9	+108	6.59 ± 0.17	6.55				
H9	3835.4	+56	7.10 ± 0.20	7.16				
H8	3889.1	+59	6.73 ± 0.15	7.00				
Ca II	3933.7	+191	2.43 ± 0.09	2.45				IS
Hε	3970.1	+70	8.67 ± 0.16	8.56				
Hδ	4101.8	+40	8.17 ± 0.24	7.97				
Hγ	4340.5		6.28 ± 0.17	6.02				
Hγ	4340.5	+187						Nebular
He I + Fe I,II	4385		0.43 ± 0.07	0.14				
He I	4471.5	+57	0.40 ± 0.07	1.09				
Mg II	4481.1	+77	0.34 ± 0.08					
Hβ	4861.3		6.55 ± 0.14	6.08				
Hβ	4861.3	+199						Nebular
He I	4921.9	+27	0.56 ± 0.08	0.35				
[O III]	4958.9	+181	−0.36 ± 0.06					Nebular
[O III]	5006.8	+164	−0.85 ± 0.05					Nebular
Mg I	5170		0.76 ± 0.12	1.20[b]				
Mg I	5185.5	+23	0.43 ± 0.10					
Fe I + Ca I	5270		0.40 ± 0.04	0.57[b]				
Cr I + Cu I	5782		0.75 ± 0.08	0.32		1.09 ± 0.17	2.53	
Na I	5890.0	+193	6.20 ± 0.10	6.49	+200	6.59 ± 0.18	6.74	IS
Na I	5895.9	+183			+198			IS
	6283.9	+206	1.52 ± 0.11		+174	2.17 ± 0.22		DIB?
[O I]	6300.3	+181	−0.48 ± 0.06					Nebular
Fe I + Ba II + Ca I	6497		0.79 ± 0.07	0.52		0.82 ± 0.16	0.71	
[N II]	6548.0	+111	−1.34 ± 0.05		+80	−0.86 ± 0.08		Nebular
Hα	6562.8	+104	−4.34 ± 0.05		+77	−6.05 ± 0.08		Nebular
[N II]	6583.4	+108	−3.59 ± 0.05		+61	−2.98 ± 0.09		Nebular
[S II]	6716.5	+126	−1.34 ± 0.06		+65	−1.57 ± 0.09		Nebular
[S II]	6730.9	+121	−1.10 ± 0.06		+61	−1.14 ± 0.09		Nebular
Ti I + Fe I	8468		0.54 ± 0.08			0.60 ± 0.08		
Ca II	8498.0	+31	1.43 ± 0.13[c]		+133	1.21 ± 0.14[c]		
Fe I + Ti I	8516		0.41 ± 0.08			0.83 ± 0.09		
Ca II	8542.1	+36	4.09 ± 0.13[c]		+126	4.14 ± 0.14[c]		
Pa 14	8598.4		1.51 ± 0.16					
Ca II	8662.1	+38	4.41 ± 0.13[c]		+135	4.75 ± 0.14[c]		
Fe I	8688.6	+38	0.36 ± 0.06		+137	0.51 ± 0.07		
Pa 12	8750.5		2.56 ± 0.16	2.45		2.16 ± 0.18	2.30	

[a] All windows as defined by Bica & Alloin (1986) except for the following:
[b] Windows as defined by Faber et al. (1985).
[c] Equivalent widths measured using the bands defined by Diaz, Terlevich & Terlevich (1989).

DIBs are reviewed by Herbig (1995). The strongest DIBs in the optical spectral region are the λλ5778–80, 6283 and 6533 features, and we therefore looked for these in our spectra. The λ5778–80 feature is coincident with the λ5782 Cr I + Cu I blend, which we positively identify in the spectra of F and L. The λ6283 DIB is, however, probably present. We see a weak feature at 6288 Å (see Table 2), which is definitely real as it occurs in the overlap region between spectra and is seen in both sets of data. Comparison with the spectral library of Jacoby et al. (1984) shows that it does not appear to be a stellar absorption feature. Likewise, comparison with the sky spectrum and the atmospheric standard shows that it is not due to oversubtracted sky or a telluric feature. The strength of the λ6288 absorption also correlates with reddening, being stronger in cluster L, as expected if this is a DIB. The possibility therefore remains that the feature at λ6288 could be a DIB arising from the interstellar medium of M82.

The absorption strengths of DIBs are complicated. They are usually strongest in the boundaries of molecular clouds and tend to weaken in purely molecular regions as well as being absent from H II regions (e.g. Jenniskens, Ehrenfreund & Foing 1994). This behaviour is consistent with models where DIBs are produced by ionized large molecules (Sonnentrucker et al. 1997). Typical Galactic paths with $E(B-V) \approx 1$ produce central absorption depths of ≈0.75 in the λ6283 DIB (e.g. Jenniskens & Desert 1993; Herbig 1995), slightly stronger than what we observe in either cluster F [$E(B-V) \approx 1$–1.5] or cluster L [$E(B-V) \geq 2$] in M82. The modest strengths of the DIBs along paths through the M82 interstellar medium (ISM) which contains strong Na I D lines

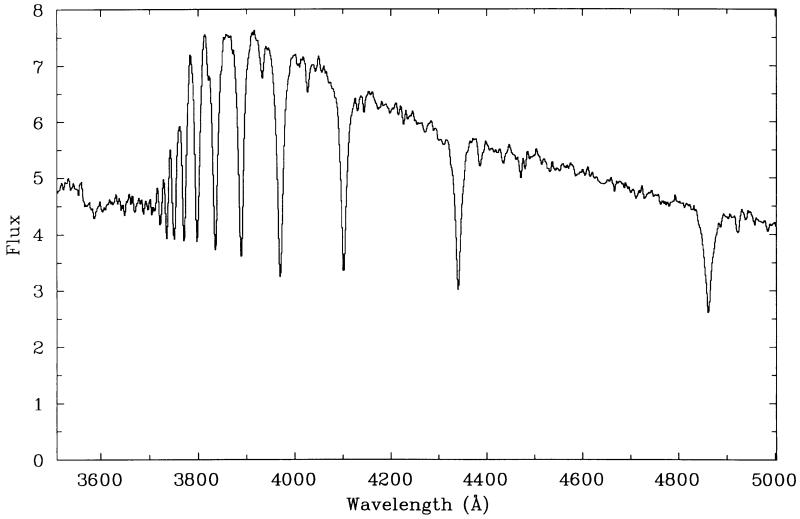

Figure 4. This plot shows the model spectrum for a star cluster with an age of 60 Myr computed with PEGASE. The flux is in units of erg s^{-1} $Å^{-1}$ per solar mass of cluster where a Salpeter initial mass function was assumed. The spectrum was synthesized using the Jacoby et al. (1984) library of stellar spectra and Geneva stellar evolution tracks.

and thus neutral gas suggests that we are observing these two clusters through regions with few ionization boundaries. In this case we might expect small-scale structure to be common in the ISM, which could contribute to non-uniform interstellar obscuration across the faces of the clusters. Follow-up observations are needed to establish whether M82 is the second galaxy outside of the Local Group where DIBs have been detected (the first being supernova 1986G in NGC 5128; see Herbig 1995).

4 COMPARISONS WITH THEORETICAL STAR CLUSTER MODELS

4.1 Blue wavelength region

Quantitative models now exist for spectra of single-age, solar-metallicity star clusters that formed over short time-scales. We used the results from the spectral synthesis code 'Projet d'Etude des Galaxies par Synthèse Evolutive' (PEGASE; Fioc & Rocca-Volmerange 1997). These models are well suited to our needs because they include supergiant stars that are critical in the spectra of young star clusters; models that exclude such stars will not give proper matches to integrated spectra of younger super star clusters (e.g. Brodie et al. 1998). We selected the 'Geneva' stellar evolution tracks from Schaller et al. (1992) and Charbonnel et al. (1996) in computing cluster models with PEGASE.

PEGASE also offers a choice of spectra synthesized from relatively low spectral resolution model atmospheres, or the Jacoby et al. (1984) spectrophotometric library. We chose the latter option for this project, as the near-solar metallicity should be a reasonable match to young objects in M82, and we desired the best possible spectral resolution. Even though this still appears to be the highest spectral resolution Galactic spectrophotometric library that includes a wide range of spectral and luminosity classes, it has lower resolution (4.5 Å), and often lower per-pixel signal-to-noise ratios, than our WHT spectra of M82 cluster F. Improved spectral libraries will be important for future comparisons between model and observed spectra of nearby SSCs.

Before comparing with blue-region spectra of model star clusters, we smoothed the cluster F spectrum with a Gaussian having $\sigma = 1.0$ pixel over λλ3510–5002 Å. This slightly degrades our resolution to about 2 Å. We also shifted the observed spectrum by -175 km s^{-1} to account for the approximate redshift of the stellar absorption lines. The IRAF package SARITH was then used to make ratios between the wavelength- and flux-calibrated data and lower spectral resolution blue-region PEGASE models. Models were computed for ages of 20, 40, 60, 80 and 100 Myr with a Salpeter IMF. The best-fitting 60 Myr model blue-region spectrum is shown in Fig. 4.

The comparisons between PEGASE models and data are very good. Ratios between observations and model spectra reveal both components of the interstellar H and K Ca II absorption lines, as well as fainter Balmer emission from the Hγ and Hδ lines. Some 'ringing' is present among the higher Balmer series, probably resulting from the modest spectral resolution of the spectral library as well as mismatches between wavelength scales.

The ratios of spectra display an upward slope towards the red caused by dust obscuration in M82. OM78 estimated the reddening towards cluster F to be $E(B-V) \approx 1$; our model fits suggest a slightly higher value of $E(B-V) \approx 1.5$. However, a standard Galactic extinction model does not properly correct the data; this law has too much curvature in the near-UV. There is likely to be dust near cluster F and possibly even patchy obscuration (cf. conditions in the starburst nucleus of NGC 253; Watson et al. 1996), so it is not surprising that the Galactic extinction model fails (see also Calzetti 1999). Because of this uncertainty in the proper choice of an obscuration correction, we cannot use the continuum spectral energy distribution at optical wavelengths to determine the age of the cluster.

Our efforts therefore concentrated on matching the Balmer absorption lines and gravity/temperature-sensitive Balmer jump as the basis for selecting best-fitting models. While the models do not perfectly reproduce our observations, they do not display gross difficulties of the type encountered by Brodie et al. (1998) in their efforts to fit blue spectra of SSCs in NGC 1275. We therefore had no need to invoke an unusual form of the initial mass function; this cluster is fitted adequately with a Salpeter IMF. The 40-Myr PEGASE model gives the best fit to the Hβ, Hγ and Hδ absorption lines but does not do as well for the Balmer jump region as the 60- and

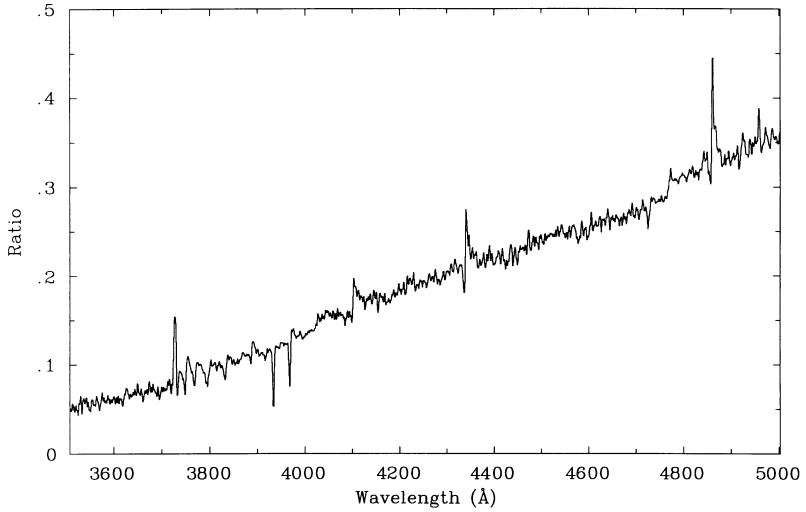

Figure 5. The ratio is plotted between the observed cluster F blue spectrum and 60 Myr PEGASE model displayed in Fig. 4. The ratio gives a model-dependent estimate for the mass of the cluster required to provide the observed flux, and in the absence of dust obscuration should be a constant function of wavelength. This ratio is normalized such that a ratio of 1 would correspond to a model cluster mass of 1.6×10^6 $M_\odot$.

80-Myr models. The 20- and 100-Myr cluster models gave worse fits in all areas. We therefore adopt an age for cluster F of 60 ± 20 Myr from the PEGASE model fitting.

The ratio between the observed cluster F spectrum and 60-Myr model is shown in Fig. 5. Since we are comparing a monochromatic luminosity with a predicted luminosity per unit cluster mass, the ratio is in units of solar masses. The normalization leads to a ratio of 1 in the plot corresponding to a cluster mass of 1.6×10^6 $M_\odot$. If we correct by a factor of 40–200 for $A_B = 4$–6 mag, then we see that a model cluster mass of $>10^7$ $M_\odot$ is needed to reproduce the blue luminosity. Because the form of the initial mass function in SSCs is poorly known, this mass is highly uncertain. However, it does indicate that cluster F is likely to be very massive, in agreement with results from earlier studies (OM78; O'Connell et al. 1995).

4.2 Red wavelength region

The prime diagnostic for measuring ages in the red part of the spectrum is the strength of the Ca II triplet (CaT). The presence of a strong CaT is often used as an indicator of red supergiants (RSG) and therefore an age of 10^7 yr. The CaT is, however, strong in yellow supergiants as well, and, as discussed by Mayya (1997), is *not* an unambiguous signature of RSGs. Mayya (1997) finds that, at solar metallicity, the evolution of the strength of the two strongest members of the CaT (Ca2 + Ca3) shows two peaks – one from RSGs at $\sim10^7$ yr ($W_\lambda \approx 11$ Å), and one at 60 Myr from red giants and asymptotic branch stars ($W_\lambda \approx 7$ Å).

In M82 clusters F and L, the combined equivalent widths of Ca2 + Ca3 are 8.5 and 8.9 Å respectively, uncorrected for Paschen line absorption. Spectral synthesis models (Leitherer, private communication) at ages of 40–80 Myr predict equivalent widths of 7.9–8.3 Å (including the Paschen lines) and 5.6–5.9 Å (pure CaT). The strength of the CaT in the spectrum of SSC F is therefore in accord with the age deduced from the blue spectrum of ≈60 Myr. For SSC L, the only potential age information that we have is the strength of the CaT. The similarity in the strength of this feature, and the overall spectral appearance, indicates that SSC L is probably of a similar age to F.

5 DISCUSSION

The combination of high-quality optical spectra and good spectral synthesis models for star clusters has allowed us to derive an age for M82 SSC F. Since SSCs are hallmarks of episodes of intense star formation (see Hunter, O'Connell & Gallagher 1994; O'Connell et al. 1994; Watson et al. 1996), cluster F provides one benchmark in the history of the M82 starburst. While this is only one star cluster, it is a massive object, and so its birth would likely have been noticeable on a galactic scale; the star formation rate (SFR) for making this cluster during a ≈1 Myr dynamical time-scale would have been >1 $M_\odot$ yr^{-1}. Thus our data suggest a *minimum* age for the starburst in M82 of 40 Myr and a most probable age of ≥60 Myr.

Ages of the M82 starburst have been previously derived from integrated spectra of the central regions of this galaxy by Rieke et al. (1993). Their preferred models consist of two bursts within the past ∼30 Myr, each with a duration of about 5 Myr. Doane & Mathews (1993) based their models on the energetics of the stellar populations, including supernova rates estimated from radio observations, and found that the starburst has been active for 30–60 Myr. Satyapal et al. (1997) observed 12 luminous concentrations within the central starburst in the infrared (IR). They identify these objects with embedded SSCs, whose frequent presence is also required to fit the numbers of radio supernovae remnants (Golla, Allen & Kronberg 1996). The ages of these SSCs with high near-IR luminosities are estimated by Satyapal et al. (1997) to be near 10 Myr, and they present a model in which the starburst has propagated outwards from the nucleus during this time period.

At larger radii there is evidence that the starburst is older. For example, Shen & Lo (1995) measured a change in the properties of the molecular medium between the central and mid-disc zones of M82. The molecular gas at a radius of 390 pc is much more disturbed than that in the inner 125-pc region, suggesting that the outer gas was disrupted by an earlier starburst. They identify this with the 30-Myr starburst event suggested by Rieke et al. (1993). OM78 also noted that the outer region is probably an older event than that in the centre.

The structure of M82 is an important factor when discussing the 'age' of the starburst (see Telesco 1988). Cluster F lies to the

south-west of the M82 nucleus, slightly above its very heavily obscured mid-plane (Larkin et al. 1994). The rapid variation in extinction across this area is also illustrated by the presence of the highly reddened SSC L near cluster F. It is in the region of M82 where the near-IR surface brightness remains roughly constant, and may be associated with a ring structure that is inferred to surround a central bar (see Telesco et al. 1991; Larkin et al. 1994; Achtermann & Lacy 1995).

We can also use the measured radial velocities of the absorption and emission lines in the spectra of clusters F and L to obtain information on their locations within M82. Götz et al. (1990) and McKeith et al. (1993) present detailed studies of the structure of the disc of M82 using optical and near-IR emission and absorption-line velocities. In common with previous studies, they find that the size of the rotational velocity gradient increases with wavelength because of the obscuration in M82. The heliocentric velocities we derive for the interstellar absorption lines ($+189 \pm 5\,\mathrm{km\,s^{-1}}$) and the blue nebular emission lines ($+181 \pm 12\,\mathrm{km\,s^{-1}}$; Section 3.3) agree well with those determined for the same lines near the position of cluster F by Götz et al. (1990). These velocities are below the systemic value, but well above the rotation velocity in this region of M82 (e.g. Weliachew, Fomalont & Greisen 1984; Achterman & Lacy 1995), consistent with a model where the emission lines originate in ionized gas located on the near side of the outer disc of M82 (McKeith et al. 1993).

In contrast, the radial velocity of $+35$ km s^{-1} we derive for cluster F is very near the expected rotation curve peak at its position. Cluster F therefore should be located near the mid-point of our sightline through the disc of M82, at a radial distance of about 440 pc from the nucleus, near the edge of the dense gaseous ring. Possibly a hole in the dust layer is allowing us to see cluster F relatively deep within M82 (see Larkin et al. 1994). For cluster L, we find a CaT velocity of $+131\,\mathrm{km\,s^{-1}}$, which is similar to our red H II region emission-line velocities and those of Götz et al. (1990). This suggests that L is located towards the outer edges of the disc at a radius of somewhat more than 440 pc in a region of high obscuration.

The different ages derived for the M82 starburst then may simply reflect variations of the star formation history within this extraordinary galaxy. If we assume that cluster F is a typical component of the 'ring' or mid-disc, then the starburst occurred in this region rather long ago, and in the last 20–30 Myr has become more concentrated in the central part of the galaxy, where a strong bar may be present. This model is consistent with previous results in suggesting the earlier M82 starburst occurred in the mid-disc, and the more recent event is more centrally concentrated. Age dating of a larger population of star clusters beyond the currently active central-region starburst has the potential to provide a clearer view of the development of the M82 starburst.

6 CONCLUSIONS

We have obtained high signal-to-noise ratio optical spectra with good wavelength resolution for star clusters F and L in M82. Quantitative fits to theoretical models are successful in reproducing the spectra with an SSP having an age of $\approx$60 Myr for cluster F. This corresponds to a main-sequence turn-off mass of about $7\,\mathrm{M_\odot}$, consistent with the temperatures of stars associated with weaker spectral lines seen in the blue region. Cluster L appears to have a similar age, but the result is much less certain because of the lack of blue spectra. The combination of high-quality spectra and stellar population models that include supergiant stars provides a powerful means to analyse young super star clusters.

Combining our estimate of $V = 15.8$ with an extinction of $E(B-V) \approx 1.5$ we derive $M_V = -16.5$ for cluster F, two magnitudes brighter than that determined by O'Connell et al. (1995). It therefore appears likely that these clusters are extremely massive and may have the ability to survive as bound systems over long time-scales (e.g. Goodwin 1997). A measurement of the stellar velocity dispersion in cluster F would be extremely useful in constraining its mass and thus similarity to globular star clusters as well as future evolution (cf. Ho & Filippenko 1996).

The spectra indicate that while cluster L is more obscured than cluster F, the latter star cluster likely lies near the outer edge of the main starburst region in M82. It is an extremely luminous super star cluster, whose presence strongly suggests that the M82 starburst was quite active 60 Myr ago. These clusters also offer useful test paths through the ISM of M82, and in addition to the well-known atomic absorption of Na I D and Ca II H+K, we find a probable DIB feature.

ACKNOWLEDGMENTS

We thank Claus Leitherer for providing model equivalent widths of the Ca II triplet lines. We especially thank the staff of the Royal Greenwich Observatory for obtaining the observations of M82 for us through the service programme. The William Herschel Telescope is operated on the island of La Palma by the Royal Greenwich Observatory in the Spanish Observatorio del Roque de los Muchachos of the Instituto de Astrofísica de Canarias.

REFERENCES

Achtermann J. M., Lacy J. H., 1995, ApJ, 439, 163
Andrillat Y., Jaschek C., Jaschek M., 1995, A&AS, 112, 475
Arp H., Sandage A., 1985, AJ, 90, 1163
Bica E., Alloin D., 1986, A&A, 162, 21
Brodie J. P., Schroder L. L., Huchra J. P., Phillips A. C., Kissler-Patig M., Forbes D. A., 1998, AJ, 116, 691
Bruzual G., 1996, in Leitherer C., Fritze-von Alvensleben U., Huchra J., eds, ASP Conf. Ser. Vol. 98, From Stars to Galaxies: The Impact of Stellar Physics on Galaxy Evolution. Astron. Soc. Pac., San Francisco p. 14
Bruzual G., Charlot S., 1993, ApJ, 405, 538
Calzetti D., 1999, XXXIIIrd Recontres de Moriond on Dwarf Galaxies, in press (STScI Preprint No. 1262)
Carquillat J. M., Jaschek C., Jaschek M., Ginestet N., 1997, A&AS, 123, 5
Charbonnel C., Meynet G., Maeder A., Schaerer D., 1996, A&AS, 115, 339
Colbert J. W. et al., 1999, ApJ, in press
Conti P. S., Vacca W. D., 1994, ApJ, 423, L97
Diaz A. I., 1988, MNRAS, 231, 57
Diaz A. I., Terlevich E., Terlevich R., 1989, MNRAS, 239, 325
Doane J. S., Mathews W. G., 1993, ApJ, 419, 573
Faber S. M., Friel E., Burstein D., Gaskell C. M., 1985, ApJS, 57, 711
Fioc M., Rocca-Volmerange B., 1997, A&A, 326, 950
Freedman W. et al., 1994, ApJ, 427, 628
Golla G., Allen M. L., Kronberg P. P., 1996, ApJ, 473, 244
González Delgado R. M., Leitherer C., Heckman T. M., 1997, ApJ, 489, 601
Goodwin S. P., 1997, MNRAS, 286, 669
Götz M., McKeith C. D., Downes D., Greve A., 1990, A&A, 240, 52
Herbig G. H., 1995, ARA&A, 33, 19
Ho L. C., 1997, Rev. Mex. Astron. Astrofis. Ser. Conf., 6, 5
Ho L. C., Filippenko A. V., 1996, ApJ, 472, 600
Horne K., 1986, PASP, 98, 609
Hunter D. A., O'Connell R. W., Gallagher J. S., III, 1994, AJ, 108, 84
Jacoby G. H., Hunter D. A., Christian C. A., 1984, ApJS, 56, 257
Jenniskens P., Desert F. X., 1993, A&AS, 106, 39

Jenniskens P., Ehrenfreund P., Foing B., 1994, A&A, 281, 517
Kronberg P. P., Pritchet C. J., van den Bergh S., 1972, ApJ, 173, L47
Lamb S. A., Gallagher J. S., III, Hjellming M. S., Hunter D. A., 1985, ApJ, 291, 63
Larkin J. E., Graham J. R., Matthews K., Soifer B. T., Beckwith S., Herbst T. M., Quillen A. C. 1994, ApJ, 420, 159
Lynds C. R., Sandage A. R., 1963, ApJ, 137, 1005
McKeith C. D., Castles J., Greve A., Downes D., 1993, A&A, 272, 98
Mayya Y. D., 1997, ApJ, 482, L149
Meurer G. R., Heckman T. M., Leitherer C., Kinney A., Robert C., Garnett D. R., 1995, AJ, 110, 2665
O'Connell R. W., Mangano J. J., 1978, ApJ, 221, 62 (OM78)
O'Connell R. W., Gallagher J. S., III, Hunter D. A., 1994, ApJ, 433, 650
O'Connell R. W., Gallagher J. S., III, Hunter D. A., Colley W. N., 1995, ApJ, 446, L1
Oke J. B., 1990, AJ, 99, 1621
Rieke G. H., Loken K., Rieke M. J., Tamblyn P., 1993, ApJ, 412, 99
Satyapal S. et al., 1995, ApJ, 448, 611
Satyapal S., Watson D. M., Pipher J. L., Forrest W. J., Greenhouse M. A., Smith H. A., Fischer J., Woodward C. E., 1997, ApJ, 483, 148
Schaller G., Schaerer D., Meynet G., Maeder A., 1992, A&AS, 96, 269
Schweizer F., Seitzer P., 1993, ApJ, 417, L29
Schweizer F., Miller B. W., Whitmore B. C., Fall S. M., 1996, AJ, 112, 1839
Searle L., Wilkinson A., Bagnuolo W. G., 1980, ApJ, 239, 803
Shen J., Lo K. Y., 1995, ApJ, 445, L99
Shortridge K., Meyerdierks H., Currie M., Clayton M., 1997, Starlink User Note 86.13, Rutherford Appleton Laboratory
Sonnentrucker P., Cami J., Ehrenfreund P., Foing B. H., 1997, A&A, 327, 1215
Telesco C. M. 1988, ARA&A, 26, 343
Telesco C. M., Campins H., Joy M., Dietz K., Decher R., 1991, ApJ, 369, 135
Vacca W. D., Robert C., Leitherer C., Conti P., 1995, ApJ, 444, 647
Watson A. et al., 1996, AJ, 112, 534
Weliachew L., Fomalont E. B., Greisen E. W., 1984, A&A, 137, 335
Whitmore B. C., Schweizer F., 1995, AJ, 109, 960
Whitmore B. C., Schweizer F., Leitherer C., Borne K., Robert C., 1993, AJ, 106, 1354
Zepf S. E., Carter D., Sharples R. M., Ashman K. M., 1995, ApJ, 445, L19

This paper has been typeset from a TEX/LATEX file prepared by the author.